DETECTION OF THE LAMINAR SUPERLAYER FROM TPIV MEASUREMENTS IN A TURBULENT JET

Nikolay Semin, Gerrit Elsinga and Jerry Westerweel
Laboratory for Aero- & Hydrodynamics
Delft University of Technology
Leeghwaterstraat 21, 2628 CA Delft, The Netherlands
n.v.semin@tudelft.nl

ABSTRACT

We study experimentally the entrainment mechanism in a turbulent round submerged liquid jet at $Re = 3.5 \times 10^3$. This is an extension of several previous works. The main difference is that we detect the turbulent/non-turbulent interface directly from the vorticity. For that, we set up a careful experiment, zooming in at the fluctuating boundary of the jet. With the Tomographic Particle Image Velocimetry, we measure the full velocity gradient tensor in multiple points with a sufficient spacial resolution. We can identify the laminar superlayer and obtain conditional flow statistics relative to it. The results allow us to reexamine the assumptions validity used in previous experimental studies with conclusions derived from them.

INTRODUCTION

Turbulent entrainment is a similarity hypothesis introduced first in 50's by Taylor and further developed by Batchelor and his co-workers (Turner (1986)). It states that the mean flow across the edge of a turbulent flow (V from the inset in figure 1) is assumed to be proportional to a characteristic velocity, usually local time-average maximum mean velocity at the level of the inflow (U_c in figure 1(a)). This simple idea turned out a very powerful tool for predicting the behavior of turbulent flows with free surfaces, such as all free shear flows (jets, plumes, wakes, mixing layers), penetrative convection, avalanches, gravity currents, etc. More broadly, the entrainment process can be regarded as a transition phenomena when practically irrotational fluid elements from the free stream flow region cross the turbulent boundary and acquire "turbulence". This perspective has raised questions what the mechanism of the process is and how it varies between different types of turbulent flows with free surfaces (Turner (1986); Corrsin & Kistler (1955)). Historically, two major views can be identified as engulfment and nibbling.

Engulfment is when large packets of fluid are drawn into the turbulent region by the inviscid action of the dominant eddies inside the turbulent flow region (Turner (1986)). Initial stage of the process is viewed as Kelvin-Helmholtz type of instability with subsequent formation of Stuart's type vortices or "cat's eye" pattern (Stuart (1967)). The vortex pairing leads to the growth of the layer. Inviscid action implies that the fluid

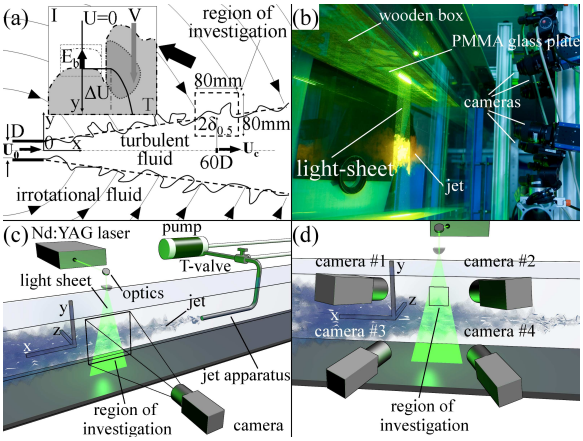

Figure 1. (a) Sketch of a turbulent jet showing the region of investigation in this study with TPIV. Streamlines pattern is based on visualizations 169-171 in Van Dyke (1982). The insert illustrates the concept of the T/NT interface separating irrotational (I) and turbulent (T) flow regions. (b) Photograph of the set-up. For the visualization, we marked the jet fluid with a rhodamine dye. It fluoresces red excited by the green laser light. (c) Schematic of the planar PIV experiment. (d) Schematic of the TPIV experiment.

packets are irrotational according to the mechanism, i.e. fluid takes part only in solid body rotation. The packets break down within the turbulent region and acquire vorticity by viscous diffusion at small-scales.

Nibbling is an outward spreading of small-scale vortices, i.e. engulfing motion on small scales. This view is based on a well known fact that in free turbulent flows such as jets, wakes and boundary layers, there is a sharp but convoluted interface between the region where the flow is turbulent and the external region of irrotational motion (Corrsin & Kistler (1955); Phillips (1972)). We refer to this boundary as a turbulent/non-turbulent (T/NT) interface (inset in figure 1(a)). This means that the boundary entrainment maybe be thought of as an interface moving through the fluid with some velocity (E_b from the inset in figure 1(a)) normal to itself. Non-turbulent or prac-

tically irrotational fluctuations here are understood as non-contributing ones to the shear stress. In the first place vorticity is acquired by a fluid element outside the T/NT interface only through the action of molecular viscosity. Once such an element has some vorticity, it can be amplified by the straining induced by the neighboring turbulence.

The engulfment can explain why the entrainment rate is independent from viscosity at high Reynolds numbers (Turner (1986)). Nibbling predicts the existence of a finite velocity jump at the T/NT interface from idealized control volume analysis for the tangential momentum due to the momentum flux balance (Corrsin & Kistler (1955); Reynolds (1972)). In 70's attempts to determine this jump via conditionally sampled hot-wire data in Turbulent Boundary Layers (TBLs) were not successful (Kaplan (1968); Kovasznay *et al.* (1970)). Contrary to the prediction, in these studies velocity appeared to be continuous across the entrainment interface.

Originally, Corrsin & Kistler (1955) came up with the idea behind nibbling. They conjectured the existence of a so-called "laminar superlayer". It is thought to bound the T/NT interface (Holzner & Lüthi (2011); Westerweel *et al.* (2011)). This is a conjunction region of local velocity gradient or a shear layer that is essentially viscous or laminar. Large eddies are straining this shear layer and keeping it thin. The layer entraps irrotational fluid into the turbulent motion via viscous force. This idea was buried under the overwhelming experimental evidence from mixing layer visualizations of Brown & Roshko (1974). They demonstrated the existence and persistence of quasi two-dimensional large coherent structures. This gave a support to the engulfment process, i.e. large-scale Reynolds shear stress. Starting from mixing layers, the mechanism was extended to jets and other free turbulent shear flows (Turner (1986); Dahm & Dimotakis (1987)). The problem here is that well-defined large-scale eddies are not ubiquitous in other types of free turbulent shear flows, except mixing layers. In particular, in jets distinct vortex rings can be unambiguously identified only within few diameters from the nozzle.

The discussion was revamped by Mathew & Basu (2002). They conducted a DNS of a circular shear-layer as a model for a developing jet at $Re_\lambda \approx 50$. The direct measurement of the engulfed volume showed that it contributed only about $10 \div 20\%$ to the growth of the jet fluid volume. Also they followed fluid parcels released in the irrotational part near the interface. If the engulfment mechanism outlined above had been dominant, then fluid elements on average would acquire vorticity already an order of magnitude further inside the turbulent flow region than in case of nibbling. The opposite was observed. This cofirmed indirectly the importance of the small-scale process at the boundary. They tried to reconcile the contradiction that the entrainment could be predicted based on large-scale quantities even though the process occurred at small-scales. For that, they stated that a fixed relationship across scales as in fully developed turbulent flows was the only requirement.

Bisset *et al.* (2002) analyzed DNS of a plane wake at $Re_\lambda \approx 50$. They used both passive scalar and enstrophy based thresholds to detect the T/NT interface. Conditional statistics relative to the T/NT interface revealed sharp jumps of the streamwise velocity component and the scalar. To inspect the flow pattern near the interface, they used sectional streamlines relative to vorticity surfaces. The conclusion was that engulfing motions were dominant and no significant nibbling was observed.

Westerweel *et al.* (2005, 2009, 2011) investigated an axisymmetric jet at $Re_\lambda \approx 50$. They used 2D PIV for vorticity measurements. However, insufficient resolution and only one vorticity component did not let them detect the interface directly. Instead, fluorescent dye and temperature field were used as passive scalars to distinguish between turbulent and surrounding fluid. The existence of a sharp jump in scalars over the interface was shown. There was evidence, though incomplete, of a similar sharp jump in the streamwise velocity component relative to the interface. The propagation velocity of the interface (E_b in figure 1(a)) was estimated from conditional statistics ($E_b \Delta U = -F_\tau$, where F_τ is the momentum flux) and compared to its estimate from the entrainment velocity ($E_b = -2\langle V \rangle$ in figure 1(a)). The match between two quantities was within the experimental error.

These studies are of relevance, because regions between turbulent and non-turbulent motion of very inhomogeneous turbulence play a critical role in many engineering and natural flows. For instance, Meinhart & Adrian (1995) discovered that zones of roughly constant streamwise velocity component can be identified in the instantaneous structure of velocity in a TBL. The maximum fluctuation within a zone is an order of magnitude smaller than the velocity jump at the border of the zone. One can hypothesize that the structure of a TBL consists of several T/NT interfaces, similar to ones bounding turbulent jets and wakes. Moreover, conventional turbulence models are based on studies of homogeneous or homogeneous isotropic turbulence. They perform notoriously badly in cases when inhomogeneity is an essential feature (e.g. clouds modeling). Typically, the model parameters should be first tuned based on some benchmark flow such as turbulent jet. Clearly, new ideas and approaches are required. Study of the T/NT might be one of them. As a first step, it is important to describe and quantify the characteristic features of these interfaces. Additional implications for conventional turbulence models are explored in Hunt *et al.* (2006); Westerweel *et al.* (2009); Holzner & Lüthi (2011).

Here we present results from an experimental study of the entrainment mechanism in a turbulent round submerged liquid jet at $Re = 3.5 \times 10^3$. The goal is to overcome two major assumptions in Westerweel *et al.* (2009). The first one is that the small-scale vorticity behaves like a passive scalar. This allowed them to detect the T/NT interface from the scalar field. The second assumption is the predominant orientation of the vorticity along the circumferential direction. This was dictated by the measurement technique (2D PIV). We want to detect T/NT interface right from the vorticity. For that, the access to the full velocity gradient tensor in multiple points with a sufficient spacial resolution is needed. We set up a careful experiment, zooming in at the fluctuating boundary of the jet. Figure 1(a) shows the region of investigation. With the Tomographic Particle Image Velocimetry, we obtain all vorticity components (Elsinga *et al.* (2006)) and resolve the flow-field down to the Kolmogorov scale. We identify the laminar superlayer and obtain conditional flow statistics relative to it.

EXPERIMENTAL SET-UP AND PROCEDURE

Jet experiments were done in a water tunnel. It consists of a 5 m long transparent PMMA test section with a width of 610 mm. The tunnel has an open surface. We installed a wooden box with a transparent window from PMMA on top of the tunnel to avoid water ripples which could affect the alignment of the laser sheet (figure 1(b)). The height of the formed test section was 540 mm. The temperature was monitored. It was within $17.8 \div 18.0$ °C during the whole measuring campaign.

The jet apparatus was constructed from a plastic tube of 13.2 ± 0.1 mm inner diameter and length of 60 diameters. The tube was reinforced to prevent it from bending by placing it inside another thicker tube of larger diameter. The jet apparatus was mounted on a frame and positioned in the middle of the test-section parallel to the walls of the water tunnel. The frame could be traversed parallel to itself along the water-tunnel. To drive the flow, we used an IWAKI MAGNET pump (single phase induction motor). The pump sucked water in from the settling chamber of the water tunnel at a constant flow rate of 0.29 liter/s. The exit of the pump was connected to a T-valve, so the outflow was separated in two hoses. One hose led back to the settling chamber. The other one supplied the jet. This way we controlled the flow rate of the jet.

No prior investigation of the flow inside the tube was done. We assumed that at Reynolds numbers above 2000, used in the work, the flow in the tube was a fully developed turbulent pipe flow. Since final measurements were done in the developed region of the jet and we were interested in the fluctuating boundary of the jet, all the differences to the flow due to the initial and boundary conditions were neglected.

Two types of experiments were done. For the general characterization of the jet flow we conducted a planar PIV experiment. For the high resolution investigation of the T/NT interface we did Tomographic PIV measurements. In both cases we employed a double-pulsed Nd:YAG laser (Spectra-Physics Quanta Ray 400mJ pulse energy; wavelength $\lambda = 532$ nm) for the illumination, LaVision Imager PRO-X cameras (PCO Sensicam 2048^2 px resolution; 14-bit dynamic range) for digital imaging, and some standard lenses to make a light sheet through the top wall of the tunnel in a planar cross-section through the jet centerline. The light sheet thickness was set with a diafragma. The flow was seeded with neutrally buoyant hollow glass spheres (3M S60, $\overline{d} = 10$ μm, $\rho = 600$ kg/m^3). Before the measurements we ran the tunnel to obtain a homogeneous distribution of tracers. All control of the laser intensity and timing, as well as the image acquisition, was done using LaVision Davis (v7.2-7.4) software. It was also used for image processing and vector field calculations. The coordinate system was defined as follows: x was positive in the downstream direction, parallel with the jet axis, y was radial, and z was normal to both x and y. (U,u), (V,v), and (W,w) stand for the instantaneous and fluctuating velocity components along x, y, and z directions, respectively.

In the planar PIV measurements, we traversed the frame with the jet apparatus to check the flow at different x/D stations. The schematic of the experimental set-up is shown in figure 1(c). The region of investigation was symmetrical in a planar cross-section through the jet centerline (figure 1(c)). The imaging was performed by means of a single camera with a 35mm Nikon lens, resulting in a field of view of about 300×300 mm at a mean observation distance of 2 m. For calibration of the imaging system, a type 31 calibration plate, supplied by LaVision GmbH, was used. The plate was 310×310 mm square. The RMS deviation between fitted and measured mark positions was 0.2 pixel. The light sheet thickness was set 3 mm. The delay between the two laser pulses was adjusted in such a way that the maximum particle displacement was about 10 pixels or 1.5 mm, and that the loss of particle images by out-of-plane motion was acceptable. Five hundred double-frame particle images per each station were taken. The images were evaluated in a region of 100×300 mm by 32 x 32 pixels interrogation windows corresponding to a spatial resolution of 2.45 mm in x- and y-direction. Amount of outliers was less than 5%.

For the TPIV measurements, the center of the measurement domain was positioned at the distance of $2 \times \delta_{0.5}$ from the centerline of the jet. Previous studies by Westerweel *et al.* (2009) showed that the maximum of the p.d.f. of the interface location roughly was there. The RMS is $0.4\delta_{0.5}$. Figure 1(a) shows the sketch of the experiment. At $x/D = 60$ the jet half width $\delta_{0.5} \approx 80$ mm. The reason why this location was chosen for the TPIV measurements is explained in the next section. Based on an empirical estimate for the dissipation rate in a jet from Panchapakesan & Lumley (1993), we expected the Kolmogorov scale $\eta_K \approx 0.75$ mm. The Taylor scale was found with the Taylor's expression for the dissipation rate (Davidson (2004)) $\lambda_T \approx 13.5$ mm. With the region of investigation about 80×80 mm and a final 48^3 voxels interrogation box for the vector field calculation, we expected the resolution of the measurements $2\Delta x \approx 1.8$ mm, i.e. twice the Kolmogorov scale. Hence, we were confident to obtain a fully resolved flow field. In the TPIV measurements, four cameras were used with a 100mm Zeiss camera lens each. The schematic of the experimental set-up is shown in figure 1(d). Each camera was mounted on a Scheimpflug adapter. The arrangement with the cameras was installed on the outside of the water tunnel. The centers of the cameras formed the base of a square pyramid, the optical axes of the objectives being the edges of the pyramid. The solid angle was about 1.2 sr. Due to the refraction in water, the effective solid angle was $1/n^2$ smaller or about 0.7 sr, where $n = 1.33$ is the refractive index of water. The cameras were focused at a volume spanning $80 \times 80 \times 5$ mm. Because of refractions on the optical path, we observed considerable astigmatism. It adversely influenced particles images making them ellipsoidal shape of $5-7$ px. Astigmatism effects could be avoided without the use of prisms by reducing the aperture of objectives down to f# = 11.

For calibration of the imaging system, a type 11 calibration plate, supplied by LaVision GmbH, was used. The plate was 110×110 mm square. A third order polynomial was chosen as a mapping function from camera to world coordinates, linear interpolation for the out of plane component. The RMS deviation between fitted and measured mark positions for all cameras was within 0.3 px. The light sheet thickness was $4 \div 5$ mm.

Seven hundred fifty instantaneous realizations (U,V,W) of the turbulent jet were obtained. We took three sets of two hundred fifty images each at a rate of 5 Hz. This corresponds to the time separation of 0.2 s between the recordings. The large eddy turn over time at the measurement location $T \equiv \delta_{0.5}/U_c$ was about 1.6 s. Thus, the realizations were not

statistically independent. This is because in future we want to use the dataset for the Lagrangian tracking of fluid parcels in the irrotational region of the flow while they are approaching and crossing the T/NT interface similarly to Holzner *et al.* (2007).

Before the final reconstruction of the particle image volumes, a volume-self-calibration according to Wieneke (2008) was performed. The procedure revealed a misalignment error of about 4 pixels between the cameras. After applying the correction, the final accuracy improved to 0.2 px. Each reconstructed particle image volume was analyzed by local 3D cross-correlation with an iterative multi-grid volume deformation scheme reaching a final 48^3 voxels interrogation box size with 50 % overlap. The image seeding density was about 0.05 ppp. From each recording, we obtained an instantaneous three-dimensional velocity vector volume over a grid of 77 x 77 x 3 (17,787) measurement points located every 1.0 mm in all directions.

FLOW PROPERTIES AND STATISTICS

Here we present flow properties up to the second order statistics: mean and fluctuating velocity profiles across the jet. Results are shown in figures 2 and 3. The jet behaves like a wall-free jet in an infinite space till approximately $x/D = 80$. Further, we see clear influence of the boundaries: the half-widths of the jet no longer increases, the mean centerline velocity decreases faster than $1/x$, the momentum flux is no longer constant, Reynolds stresses do not tail off and get more intensified. This was expected, because in the ideal free jet the mean velocity becomes negligible around $y = \pm 2\delta_{0.5}$ from the centerline (figure 2(d)). Hence, we can estimate the width of the jet as $4\delta_{0.5}$. This is about 405 mm at $x/D = 80$, which is comparable with the height of the tunnel 540 mm.

Also, we report a back flow after $x/D = 50$ from figure 3(d) with a magnitude about $0.1U_c$. The jet acts as a pump. Due to the mass conservation, there must be some supply. When the jet hit the wall at a far distance, it created a recirculation region. It was seen as the back flow. This back flow was highly undesirable because the same turbulence was recirculated. This made the turbulent fluid and surrounding fluid not well defined and distinguishable.

Due to these reasons, we decided to do the T/NT interface measurements at the location $x/D = 60$. This was a compromise between several requirements such as: the desire to the stay at the fully-developed region or far-field of the jet, have larger integral length scale to make sure the Taylor and Kolmorogov scales were also large, stay further from the boundaries and avoid the back flow.

To estimate the accuracy of TPIV velocity measurements, we calculated the probability distributions of the normalized velocity divergence (figure 4(a)),

$$\sigma = \left(\frac{\partial U_k}{\partial x_k}\right)^2 \Big/ \left[\left(\frac{\partial U_1}{\partial x_1}\right)^2 + \left(\frac{\partial U_2}{\partial x_2}\right)^2 + \left(\frac{\partial U_3}{\partial x_3}\right)^2\right], \quad (1)$$

over all realizations. In the computation, the partial derivatives were replaced by their finite differences. The average value of σ varies between 0, if the velocity distribution is

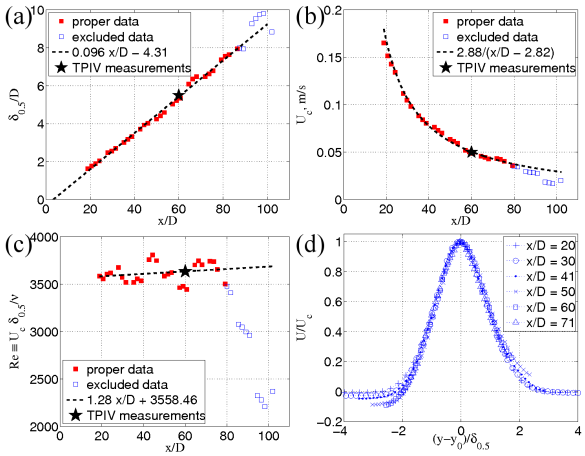

Figure 2. (a) The half-widths of the velocity field, (b) the centerline mean velocity, and (c) the corresponding Reynolds number (proportional to the square root of the total momentum flux) as functions of the distance from the nozzle. (d) Profile of the mean axial velocity at several distances from the nozzle.

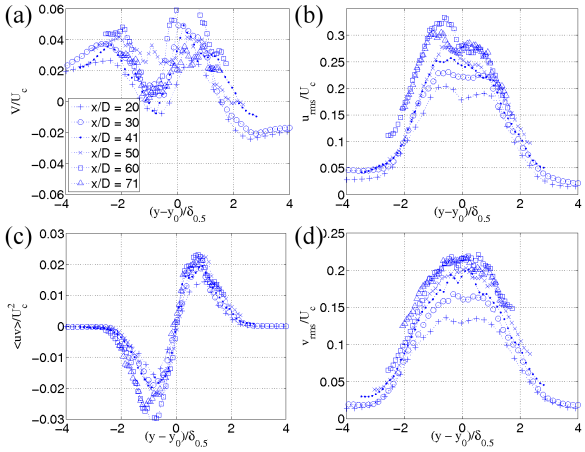

Figure 3. Profiles of the (a) mean radial velocity, (b) turbulent intensity of the axial velocity fluctuations, (c) Reynolds stress, and (d) turbulent intensity of the radial velocity fluctuations.

divergence-free, and 1 for random data. In our case $\overline{\sigma} = 0.33$. To assess the resolution of the TPIV measurements, we determined the Kolmogorov scale (η_K) from the estimated dissipation rate and the Taylor scale (λ_T) from the streamwise two-point correlation coefficient of the streamwise fluctuating velocity. The dependence of the scales on the distance from the jet centerline is shown in figure 4(b) together with the spacial resolution of the TPIV measurements and our expectations prior to the experiment. It was found that $\langle \eta_K \rangle = 0.97$ mm. Hence, the spacial resolution of the TPIV measurement (conservatively estimated as the linear dimension of the interrogation domain, i.e. 2 mm) was 2 times the Kolmogorov scale. We state that the velocity data was fully resolved.

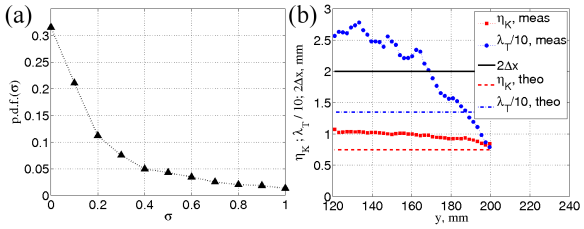

Figure 4. (a) p.d.f. of the normalized divergence, σ. (b) The Kolmogorov (η_K) and Taylor (λ_T) scales as functions of the distance from the jet centerline. Every second point is plotted. Measured values (meas) are compared with the theoretical estimates (theo) prior to the experiment and the spatial resolution ($2\Delta x$). Note that we divide λ_T by 10 for convenience of representation.

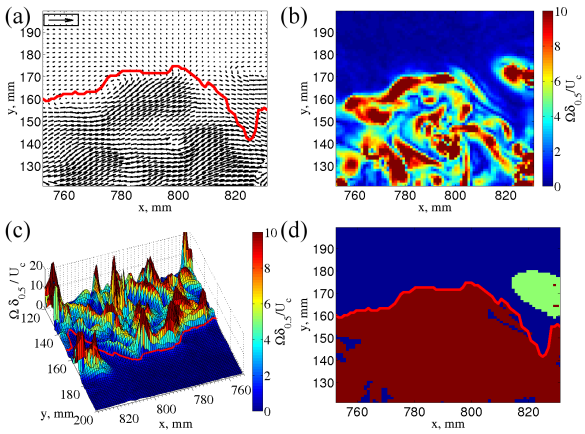

Figure 5. The detection of the interface envelope. Dimensions are in mm relative to the nozzle location (x) and the jet centerline (y). The solid red line shows the interface envelope resulting from saving the outermost points in (d).(a) Example of an instantaneous velocity field (U,V). The reference arrow in the box corresponds to a velocity of 100 mm s^{-1}.(b) Map of an instantaneous vorticity modulus.(c) Surface of the vorticity modulus.(d) Binary image obtained after applying a threshold to the vorticity modulus (b). Different colors show connected regions.

INTERFACE DETECTION

The T/NT interface was defined by using the vorticity norm $\Omega = (\Omega_i\Omega_i)^{1/2}$, where Ω_i is the vorticity field. We calculated it with the central difference method. Figure 5(a) is a typical example of an instantaneous flow-field (U,V) when the T/NT interface (the solid red line) was roughly in the middle of the measurement domain. Figure 5(b) shows the vorticity magnitude normalized with the mean centerline velocity and the jet half-width. Figure 5(c) shows the vorticity surface. It is clear that the turbulent flow is indeed surrounded by practically irrotational fluid with the vorticity RMS about $\Omega_{RMS} = 0.17U_c/\delta_{0.5}$. The vorticity undergoes a sharp jump at the interface. To determine the location of the interface, we used a threshold level within a range of $\Omega_{tr} = 0.5 \div 3U_c/\delta_{0.5}$. In this range, the interface detection did not dependent on the threshold value used. The detection threshold of $\Omega = 0.7U_c/\delta_{0.5}$ was chosen for conditional statistics in figure 6. This was exactly the same value used by Bisset *et al.* (2002); da Silva & Pereira (2008). Similar level was used by Mathew and Basu (2002).

We processed the binary image, obtained after applying the threshold, with the image processing toolbox from Matlab. Big patches of rotational fluid disconnected from the main jet flow were isolated and excluded from the processing (light green in figure 5(d)). The biggest patch of fluid was taken as the main body of the jet flow (purple in figure 5(d)). The utmost points of this patch were saved as the locations of the T/NT interface (solid red line in figure 5(d)).

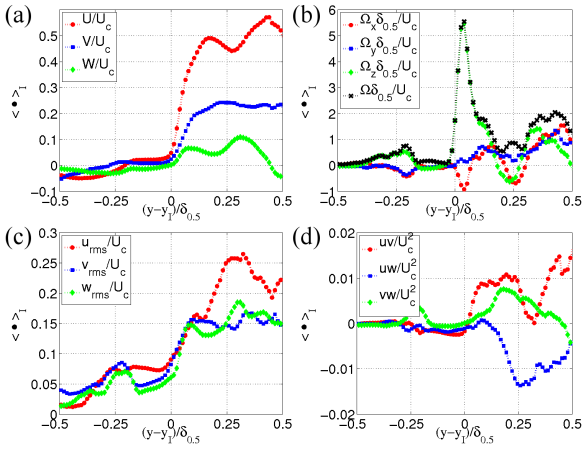

Figure 6. Conditional statistics relative to the T/NT interface location y_I. The symbol $\langle\cdot\rangle_I$ denotes the time and space average of the respective quantity. Profiles of the (a) mean velocity components, (b) mean vorticity components and vorticity norm, (c) turbulent intensities, and (d) shear Reynolds stresses.

CONDITIONAL FLOW STATISTICS

We used only velocity vector fields for statistics where the mean interface location y_I was within $\pm 0.4\delta_{0.5}$ from the center of the domain. Figure 6 shows profiles of the conditional mean velocity components, vorticity components, turbulent intensities, and shear Reynolds stresses. We denote this conditional statistics by $\langle\cdot\rangle_I$ to differentiate it from the homogeneous statistics done along the homogeneous directions of the jet.

A finite velocity jump is observed. It can be confirmed from the peak in the mean conditional vorticity in figure 6(b). The velocity jump magnitude was estimated at $\Delta U = (0.25 \pm 0.05)U_c$. Similarly, the jump in the conditional Reynolds stress was estimated at $(0.007 \pm 0.003)U_c^2$. This yields a value for the interface propagation velocity of $E_b = (0.03 \pm 0.01)U_c$. It is in agreement with the jet entrainment velocity $E = -2\langle V\rangle$. In our case, we estimate $\langle V\rangle = (-0.010 \pm 0.005)U_c$ from figure 3(a). This matches with the result from Westerweel *et al.* (2005, 2009).

The thickness of the T/NT interface was estimated $\Delta_I \approx 0.06 \div 0.07\delta_{0.5}$. Similar values were obtained in the DNS of a wake (Bisset *et al.* (2002)) and DNS of a planar jet (da Silva &

Pereira (2009)) at comparable Reynolds numbers ($Re_\lambda \approx 50$).

CONCLUSIONS

We did TPIV measurements at the fluctuating boundary of an axisymmetric turbulent jet at $Re = 3.5 \times 10^3$. Proper choice of the experimental parameters and flow conditions allowed us to fully resolve the velocity field. We detected the T/NT interface from the full vorticity vector. Making no assumption about the flow-field and interface detection, our results confirmed conclusions from previous experimental and numerical studies.

ACKNOWLEDGEMENTS

The authors wish to express their gratitude to M. Holzner, J. Mathew, C. da Silva, J.R.C. Hunt for valuable discussion on the topic. NS would like to personally thank M. Sugihto for helping with the manuscript proofreading. Financial support by FOM is gratefully acknowledged.

REFERENCES

Bisset, D.K., Hunt, J.C.R. & Rogers, M.M. 2002 The turbulent/non-turbulent interface bounding a far wake. *Journal of Fluid Mechanics* **451** (-1), 383–410.

Brown, G.L. & Roshko, A. 1974 On density effects and large structure in turbulent mixing layers. *Journal of Fluid Mechanics* **64** (04), 775–816.

Corrsin, S. & Kistler, A.L. 1955 Free-stream boundaries of turbulent flows.

Dahm, WJA & Dimotakis, PE 1987 Measurements of entrainment and mixing in turbulent jets. *AIAA journal* **25** (9), 1216–1223.

Davidson, P.A. 2004 *Turbulence: an introduction for scientists and engineers*. Oxford University Press, USA.

Elsinga, GE, Scarano, F., Wieneke, B. & Van Oudheusden, BW 2006 Tomographic particle image velocimetry. *Experiments in Fluids* **41** (6), 933–947.

Holzner, M., Liberzon, A., Nikitin, N., Kinzelbach, W. & Tsinober, A. 2007 Small-scale aspects of flows in proximity of the turbulent/nonturbulent interface. *Physics of fluids* **19**, 071702.

Holzner, M. & Lüthi, B. 2011 Laminar Superlayer at the Turbulence Boundary. *Physical Review Letters* **106** (13), 134503.

Hunt, JCR, Eames, I. & Westerweel, J. 2006 Mechanics of inhomogeneous turbulence and interfacial layers. *Journal of Fluid Mechanics* **554** (-1), 499–519.

Kaplan, R.E. 1968 The intermittently turbulent region of the boundary layer. *Tech. Rep.*. UNIVERSITY OF SOUTHERN CALIFORNIA LOS ANGELES DEPT OF AEROSPACE ENGINEERING.

Kovasznay, L.S.G., Kibens, V. & Blackwelder, R.F. 1970 Large-scale motion in the intermittent region of a turbulent boundary layer. *Journal of Fluid Mechanics* **41** (02), 283–325.

Mathew, J. & Basu, A.J. 2002 Some characteristics of entrainment at a cylindrical turbulence boundary. *Physics of Fluids* **14**, 2065.

Meinhart, C.D. & Adrian, R.J. 1995 On the existence of uniform momentum zones in a turbulent boundary layer. *Physics of Fluids* **7** (4), 694–696.

Panchapakesan, NR & Lumley, JL 1993 Turbulence measurements in axisymmetric jets of air and helium. part 1. air jet. *Journal of Fluid Mechanics* **246** (-1), 197–223.

Phillips, O.M. 1972 The entrainment interface. *Journal of Fluid Mechanics* **51** (01), 97–118.

Reynolds, WC 1972 Large-scale instabilities of turbulent wakes. *Journal of Fluid Mechanics* **54** (03), 481–488.

da Silva, C.B. & Pereira, J.C.F. 2008 Invariants of the velocity-gradient, rate-of-strain, and rate-of-rotation tensors across the turbulent/nonturbulent interface in jets. *Physics of Fluids* **20**, 055101.

da Silva, C.B. & Pereira, J.C.F. 2009 Erratum:Invariants of the velocity-gradient, rate-of-strain, and rate-of-rotation tensors across the turbulent/nonturbulent interface in jets[Phys. Fluids [bold 20], 055101 (2008)]. *Physics of Fluids* **21**, 019902.

Stuart, JT 1967 On finite amplitude oscillations in laminar mixing layers. *Journal of Fluid Mechanics* **29** (03), 417–440.

Turner, JS 1986 Turbulent entrainment: the development of the entrainment assumption, and its application to geophysical flows. *Journal of Fluid Mechanics* **173** (-1), 431–471.

Van Dyke, M. 1982 *An album of fluid motion*. Stanford, CA.

Westerweel, J., Fukushima, C., Pedersen, JM & Hunt, JCR 2005 Mechanics of the turbulent-nonturbulent interface of a jet. *Physical review letters* **95** (17), 174501.

Westerweel, J., Fukushima, C., Pedersen, J.M. & Hunt, JCR 2009 Momentum and scalar transport at the turbulent/nonturbulent interface of a jet. *Journal of Fluid Mechanics* **631** (-1), 199–230.

Westerweel, J., Petracci, A., Delfos, R. & Hunt, J.C.R. 2011 Characteristics of the turbulent/non-turbulent interface of a non-isothermal jet. *Philosophical Transactions of the Royal Society A: Mathematical, Physical and Engineering Sciences* **369** (1937), 723.

Wieneke, B. 2008 Volume self-calibration for 3D particle image velocimetry. *Experiments in fluids* **45** (4), 549–556.